## Supplemental Materials for:

# PTEN somatic mutations contribute to spectrum of cerebral overgrowth

Daniel C. Koboldt[1,2], Katherine E. Miller[1], Anthony R. Miller[1], Jocelyn M. Bush[1], Sean McGrath[1], Kristen Leraas[1], Erin Crist[1,3], Summer Fair[1], Wesley Schwind[1], Saranga Wijeratne[1], James Fitch[1], Jeffrey Leonard[4,5], Ammar Shaikhouni[4,5], Mark E. Hester[1,2,6], Vincent Magrini[1,2], Mai-Lan Ho[7], Christopher R. Pierson[8,9,10], Richard K. Wilson[1,2], Adam P. Ostendorf[2,5,11], Elaine R. Mardis[1,2,5], Tracy A. Bedrosian[1,2]

**Supplementary Table 1 Genes targeted by capture probes**

| Gene Symbol | | |
|---|---|---|
| AKT1 | FLT3 | NPM1 |
| APC | FOXL2 | NRAS |
| ATM | GNA11 | PDGFRA |
| BAP1 | GNAQ | PDGFRB |
| BRAF | GNAS | PIK3CA |
| CTNNB1 | IDH1 | PTEN |
| EGFR | JAK2 | PTPN11 |
| ERBB2 | KIT | RET |
| ESR1 | KRAS | SLC35A2 |
| FGFR3 | MPL | SMAD4 |
| | | TP53 |

# Supplemental Figures

**Supplemental Figure 1.** (**A**) Brain MRI at birth showing total hemimegalencephaly with overgrowth of the entire left cranial vault, cerebral and cerebellar hemispheres. Left cerebral overgrowth demonstrates an anteroposterior gradient of increasing severity, with the anterior frontal lobe appearing mildly enlarged, the posterior frontal and anterior temporal lobes appearing slightly disorganized and polymicrogyric, and the posterior temporal, parietal, and occipital lobes appearing severely enlarged with rightward shift and rotation of the interhemispheric falx cerebri. This includes dysplastic enlargement of the left olfactory bulb, optic pathway, basal ganglia, and hippocampal formation. Left-sided cerebral arteries and veins appeared diffusely enlarged and dysplastic, with multifocal transmantle anomalous draining veins. Aqueductal stenosis is present with triventricular hydrocephalus and excessive left ventricular enlargement proportional to cerebral hemispheric overgrowth. In addition, remote intraventricular hemorrhage was present with choroid plexus and ependymal siderosis. (**B**) Brain MRI at 14 months. There is a susceptibility artifact from a right ventriculoperitoneal shunt. Ventricular size was decreased due to shunting, except in the left posterior lateral ventricle which remains enlarged. Again demonstrated is left total hemimegalencephaly with anteroposterior gradient of overgrowth. There is more apparent transmantle dysplasia in the posterior quadrant, demonstrating full-thickness disorganized myelination with interval development of gliosis and increased conspicuity of dysplastic veins. (**C**) Micropictographs demonstrating NeuN, H&E, and SMI-32 staining of sections from brain regions A and C.

Supp. Figure 1

A.

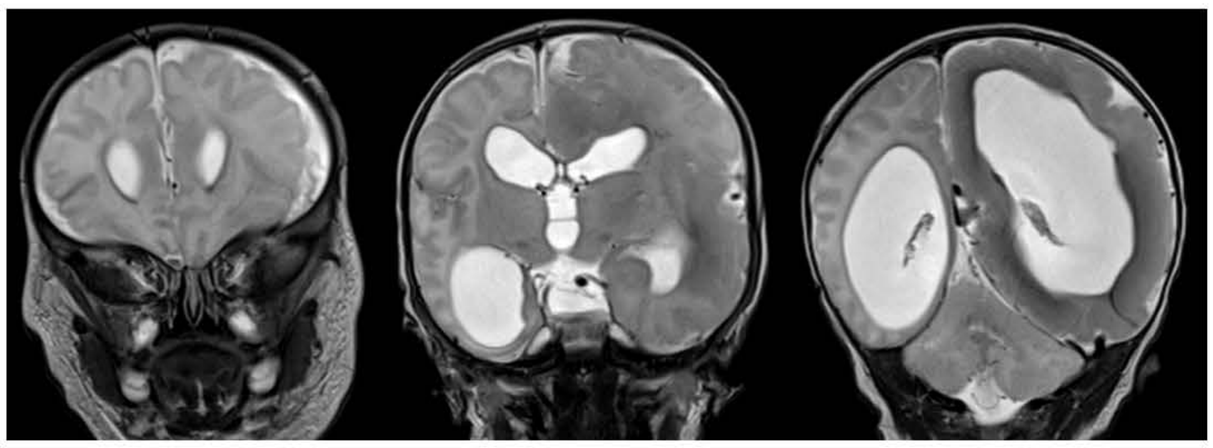

B.

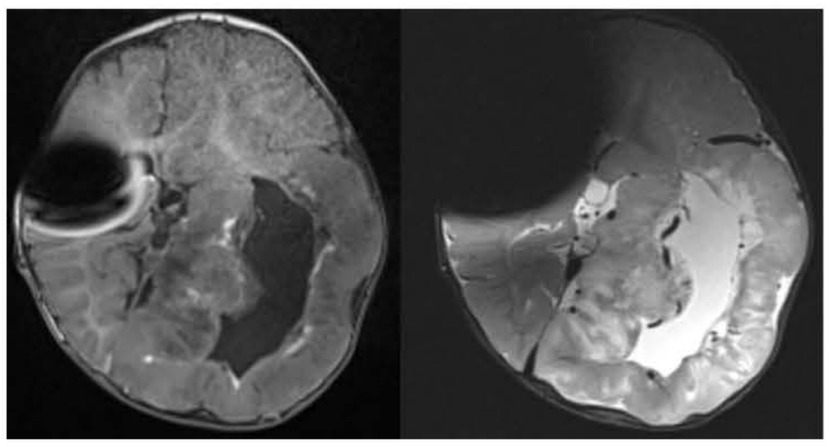

C.

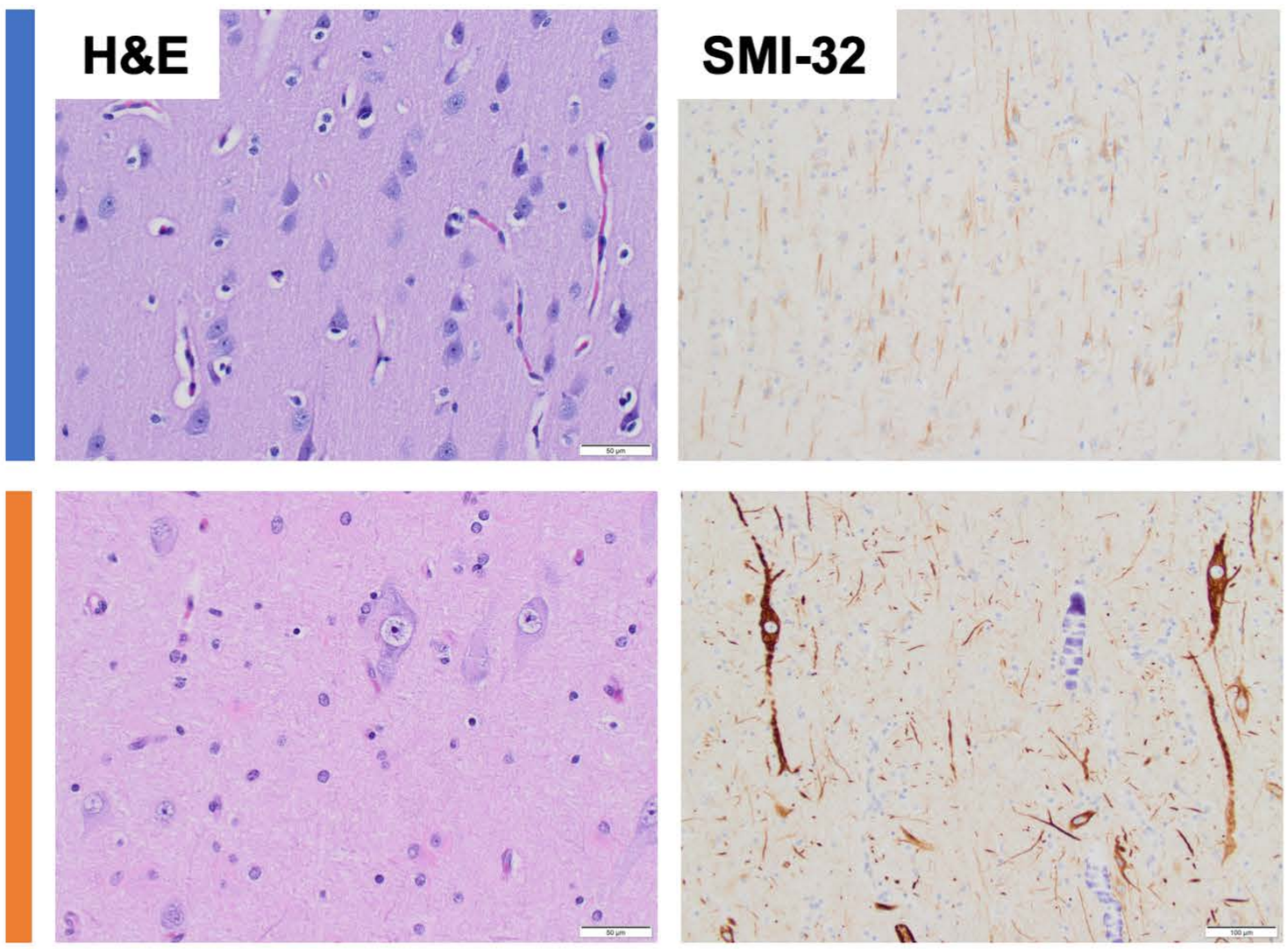

**Supplemental Figure 2.** (**A**) ExPaSY analysis of the predicted effect of each somatic mutation on the translated amino acid sequence. The exon 5 mutation is predicted to cause a premature stop codon (p.Ala86IlefsTer11), truncating the protein at 95 amino acids, whereas the exon 9 mutation causes a late stop codon (p.Asp371ValfsTer46), extending the protein to 415 amino acids instead of 403 amino acids, with residues 371-415 being different from the wild-type protein. (**B**) Total read depth obtained from targeted DNA sequencing experiments. (**C**) Sanger sequencing trace of the exon 5 variant locus in affected brain tissue, buccal cells, and blood. (**D**) Sanger sequencing trace of the exon 9 variant locus in affected brain tissue, buccal cells, and blood. (E) Split-screen IGV views of variant positions in bulk Iso-seq data.

# Supp. Figure 2

A.

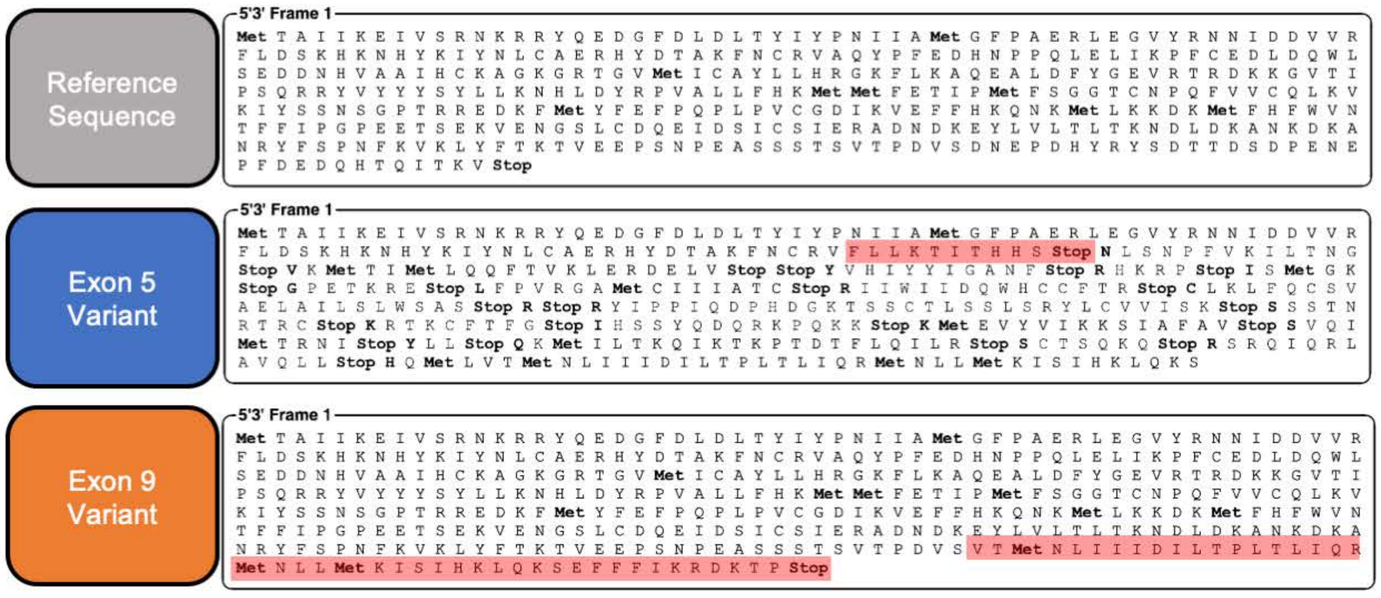


B.

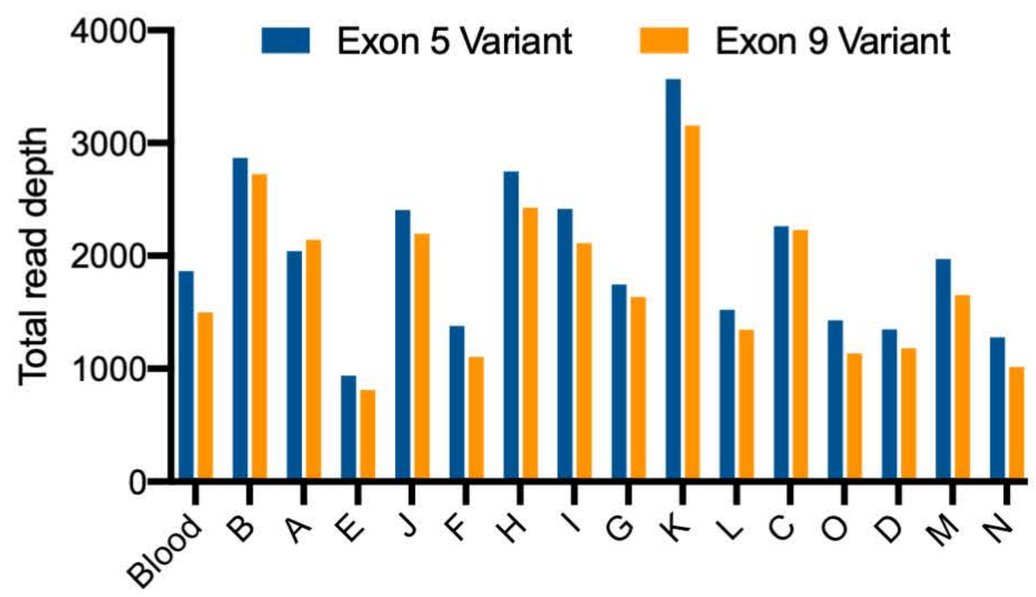


C.

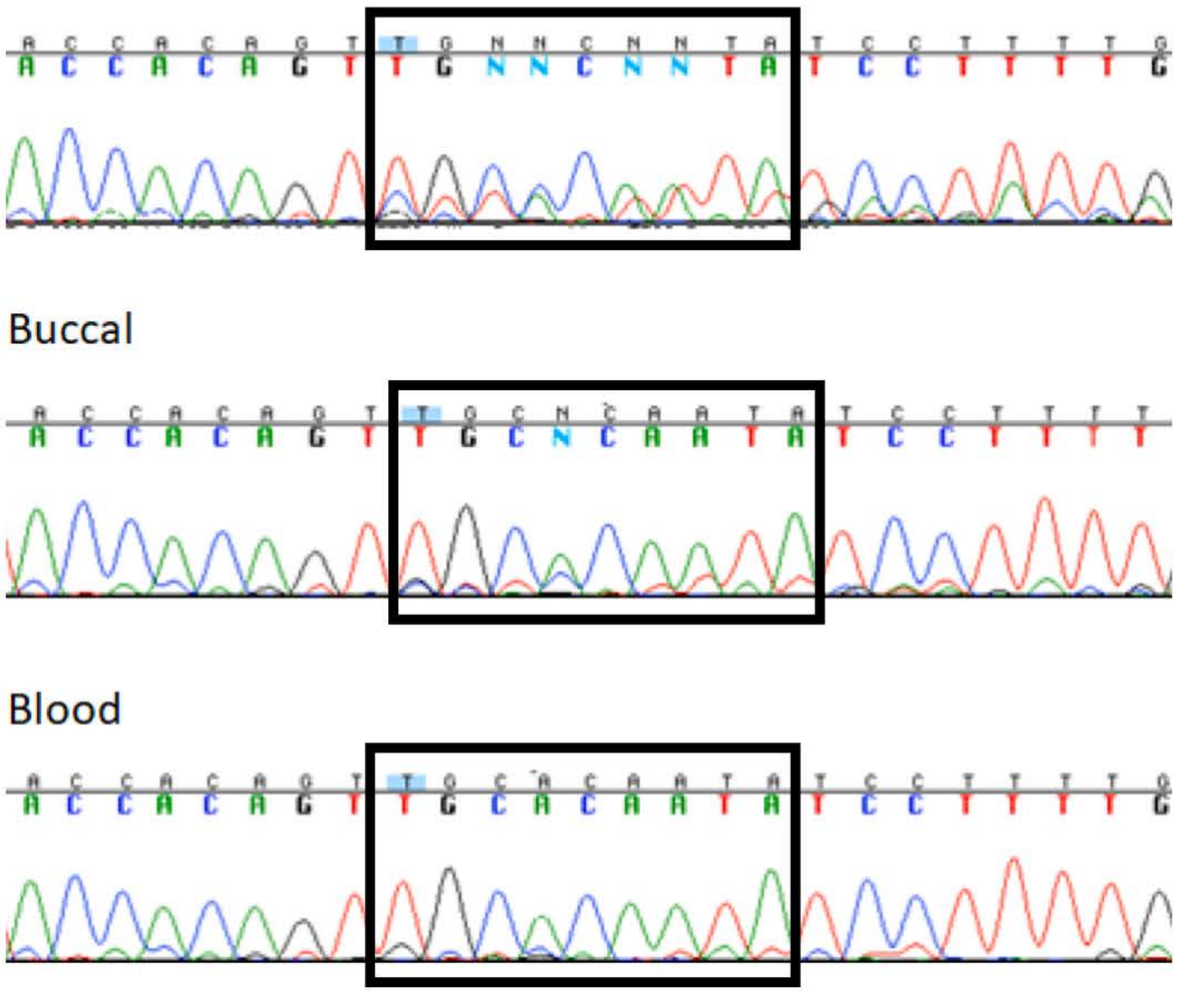


D.

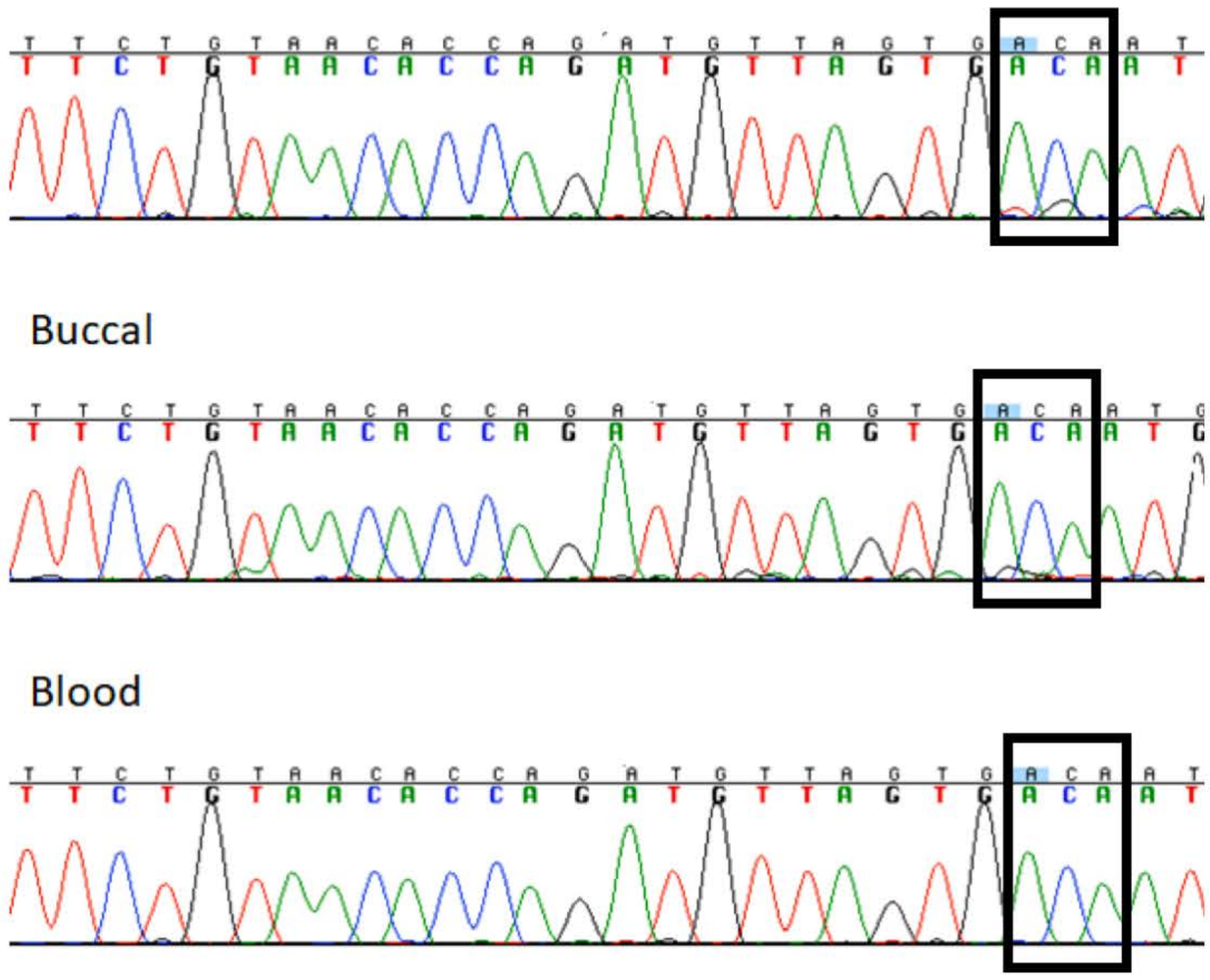


E.

**Supplemental Figure 3.** (**A**) Micropictograph showing purified Hoechst-positive nuclei and FACS analysis of nuclear scatter profiles before sorting. (**B**) Single-cell 3'-RNA-seq quality control metrics. (**C**) Top 5 differentially expressed genes for each cluster. (**D**) Top KEGG pathways in which 'Disease Involved' cluster marker genes are enriched. (**E**) Genotype status for all cells in the 3'-RNA-seq dataset. (F) UCSC genome browser views of two representative reads covering both variant positions in single-cell Iso-seq data.

# Supp. Figure 3

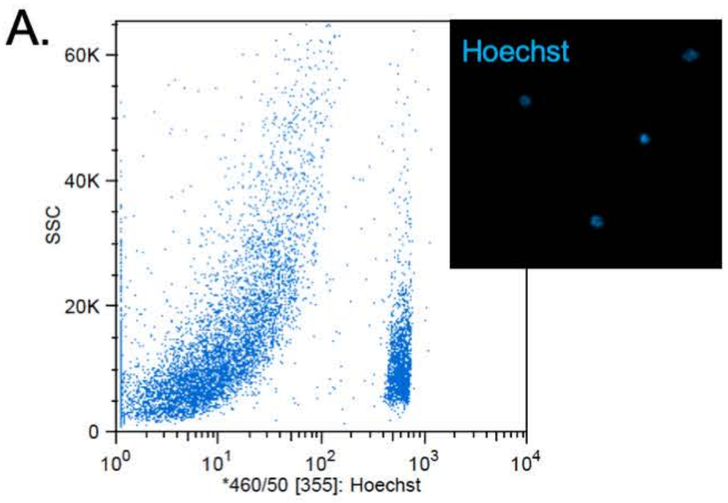


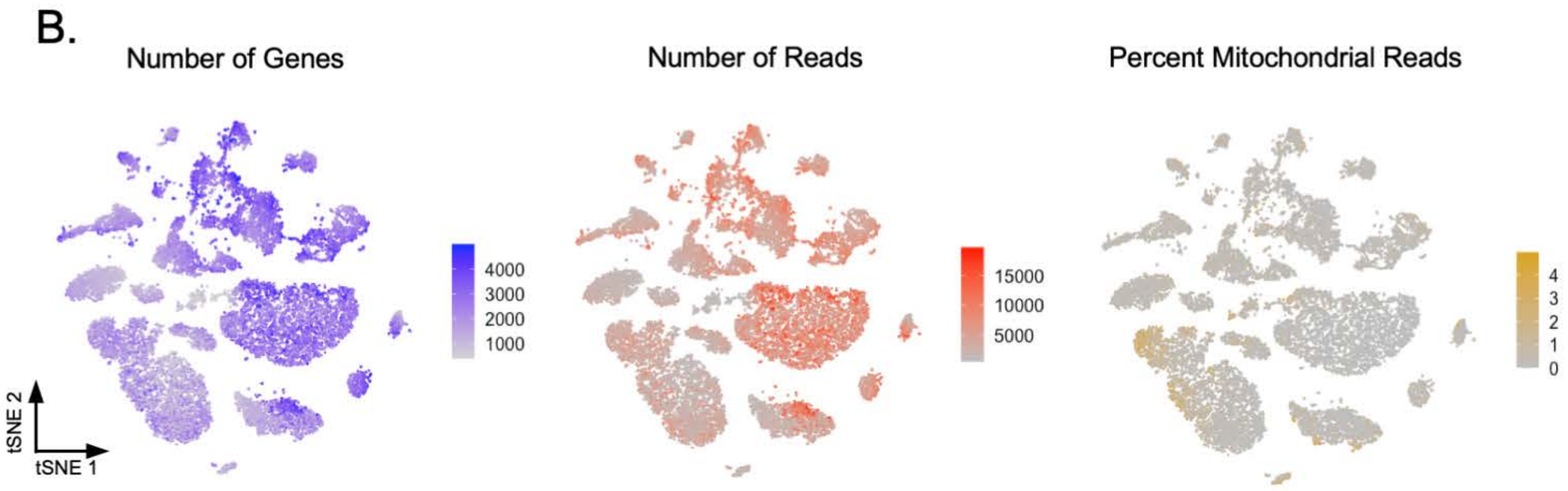


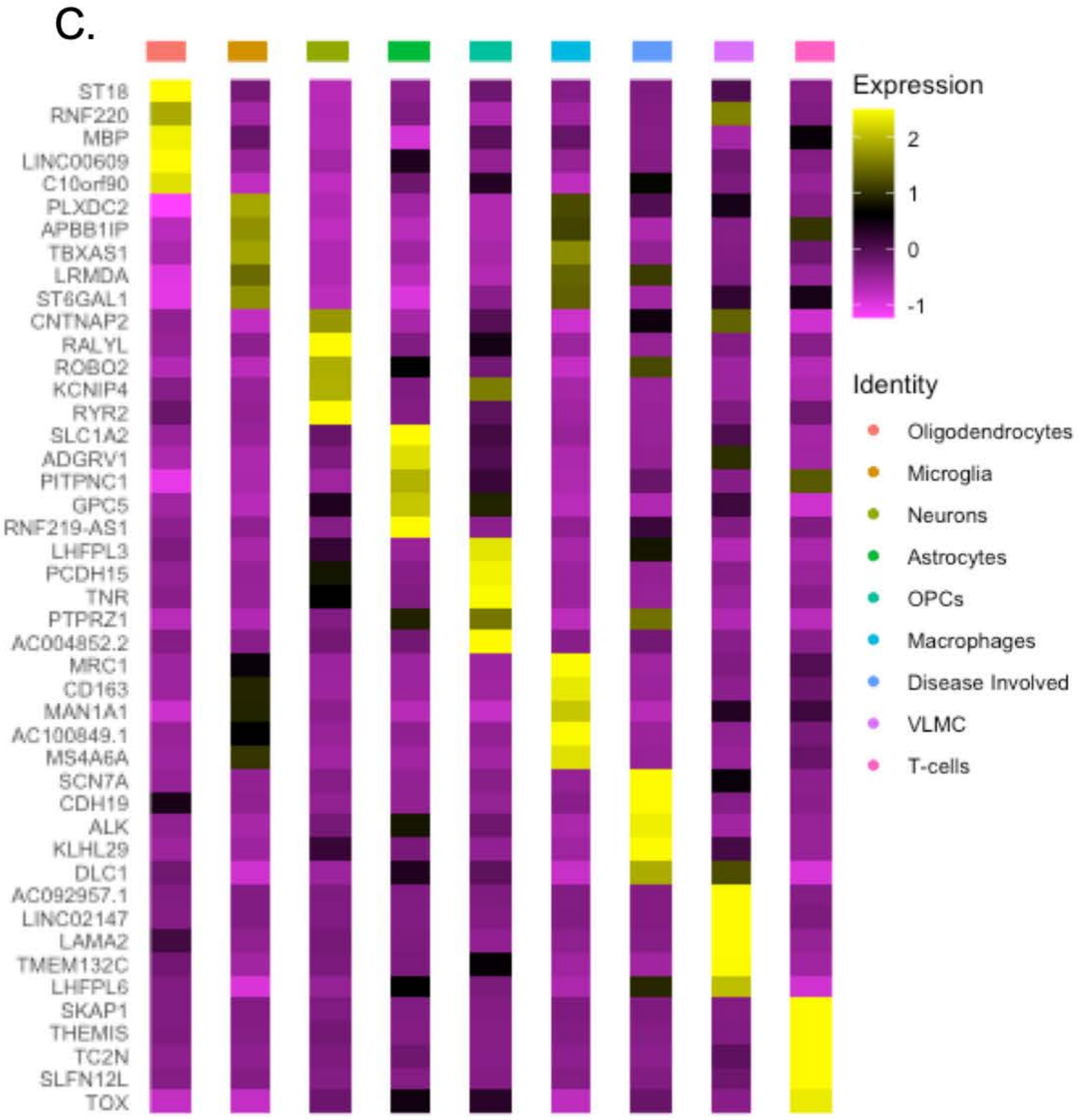


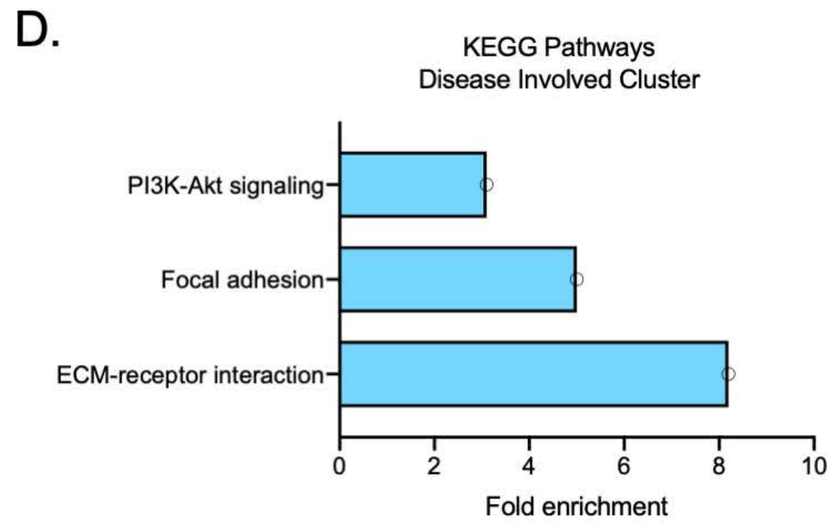


E.

| | REF | Exon 5 ALT | Exon 9 ALT | Exon 5/9 ALT/ALT |
|---|---|---|---|---|
| Oligodendrocytes | 79 | 13 | 22 | 1 |
| Microglia | 140 | 7 | 0 | |
| Neurons | 497 | 40 | 0 | |
| Astrocytes | 31 | 6 | 5 | |
| OPCs | 34 | 3 | 0 | |
| Macrophages | 11 | 1 | 1 | |
| Disease Involved | 14 | 3 | 8 | |
| VLMC | 19 | 4 | 0 | |
| T-cells | 11 | 0 | 0 | |

F.

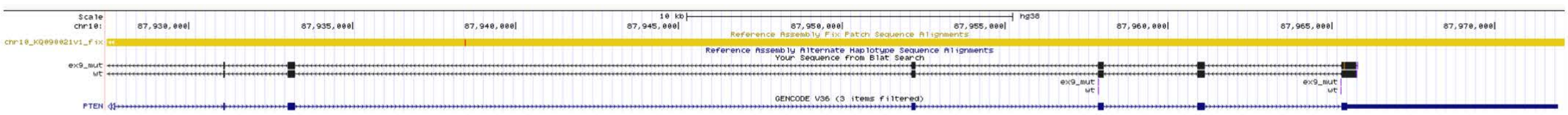

# Supplemental Text

**Case Description.** A full-term infant was born to a diabetic mother to medical attention during routine prenatal care with report of abnormal fetal ultrasound showing left hemimegalencephaly and hydrocephalus. At birth, the patient demonstrated right hemiparesis with spells characterized by right eye deviation, right arm and leg tonic extension, followed by clonic jerking of the left hemibody. Electroencephalography showed abundant multifocal epileptiform discharges, predominantly over the left hemisphere and most pronounced in the central (C3) and midtemporal (T3) head regions. In addition, there was continuous delta activity over the bo\iposterior regions that built up and became progressively synchronized prior to clinical seizures. Newborn microarray and neuronal migration gene panels were normal.

MR imaging was performed and showed total hemimegalencephaly with overgrowth of the entire left cranial vault, cerebral and cerebellar hemispheres. This included dysplastic enlargement of the left olfactory bulb, optic pathway, basal ganglia, and hippocampal formation. Left cerebral overgrowth demonstrated an anteroposterior gradient of increasing severity, with the anterior frontal lobe appearing mildly enlarged, the posterior frontal and anterior temporal lobes appearing slightly disorganized and polymicrogyric, and the posterior temporal, parietal, and occipital lobes appearing severely enlarged with rightward shift and rotation of the interhemispheric falx cerebri. Within the most severely affected posterior quadrant, there was dysplastic white matter with reduced volume and accelerated myelination. The overlying cerebral cortex showed complex sulcation with diffuse polymicrogyria and cortical thickening, with broad and shallow fused sulci producing a palisaded appearance. Left-sided cerebral arteries and veins appeared diffusely enlarged and dysplastic, with multifocal transmantle anomalous draining veins. There was evidence of Wallerian degeneration with mild atrophy of the left corticospinal tract, mammillary body, and midbrain tectum. The corpus callosum was hypoplastic and foreshortened. Aqueductal stenosis was present with triventricular hydrocephalus and excessive left ventricular enlargement proportional to cerebral hemispheric overgrowth. In addition, remote intraventricular hemorrhage was present with choroid plexus and ependymal siderosis. A

right ventriculoperitoneal shunt was placed to decompress the more normal-appearing right cerebral hemisphere.

At 3 months of age, the patient experienced his first right hemitonic-clonic seizure. Over the next year, the patient demonstrated worsening medically refractory seizures with right hemiparesis and global developmental delay. At 14 months of age, follow-up MRI was performed and again demonstrated left total hemimegalencephaly with interval progression of myelination. Ventricular size was decreased due to shunting, except in the left posterior lateral ventricle which remained enlarged. The anteroposterior pattern of left hemispheric overgrowth persisted with more apparent transmantle dysplasia in the posterior quadrant, demonstrating full-thickness disorganized myelination with interval development of gliosis and increased conspicuity of dysplastic veins.

Following discussion in a multi-disciplinary epilepsy conference, the care team elected to perform left anatomic hemispherectomy, and the patient was consented for a genomics research protocol. Sixteen representative samples were collected from the left cerebral hemisphere and submitted for pathology review as follows: A: Left Temporal Pole, B: Left Frontal Lobe, C: Left Lateral Posterior Temporal Lobe, D: Left Lateral Anterior Temporal Lobe, E: Left Frontal Pole, F: Left Frontal Lobe, G: Left Posterior Lateral Temporal Lobe, Part 2, H: Left Parietal Lobe, I: Left Medial Temporal Lobe, J: Left Anterior Frontal Lobe, K: Left Frontal Lobe, L: Left Parietal Lobe, M: Left Posterior Parietal Lobe, N: Left Posterior Parietal Lobe, O: Left Occipital Lobe, P: Left Parietal Cortex.

During pathological review, gross examination revealed a similar anteroposterior spectrum of involvement with samples from the anterior quadrant showing normal to mildly thin gyri and variable definition of gray-white matter junction (A, B, E, F, J); and posterior quadrant (C, D, G, H, I, K, L, M, N, O, P) showing thickened cortex with flattened scant sulcation and ill-defined gray-white matter junctions. On microscopic examination, sites in the left anterior quadrant showed a complex sulcal pattern with small and occasionally fused gyri, demonstrating haphazard cortical neurons with ill-defined hexalaminar architecture. Sites from the left posterior quadrant showed a flat and simplified cortical surface with thickened cortical ribbon and dysmorphic neurons. Immunohistochemical staining for GFAP showed abundant reactive astrocytes present diffusely throughout the cortex. SMI-31 and SMI-32 immunostaining labeled neuronal processes and the cell bodies of dysmorphic neurons. NeuN immunostaining revealed cortex with a paucity of neurons, all of which appeared haphazardly

situated, and loss of the expected neuronal heterogeneity seen in normal cortex. Vimentin immunostaining primarily labeled vessels and reactive elements with no unequivocal balloon cells.

Following surgery, electroencephalography showed residual disorganization and slowing within the right hemisphere. The patient has been seizure free and remains so following weaning of anticonvulsant medications. Though he still favors the left side, his right-sided strength is improving and he is making developmental gains.